

Drag reduction by polymer additives in a turbulent channel flow

By TAE GEE MIN¹, JUNG YUL YOO², HAE CHEON CHOI^{1,2}
AND DANIEL D. JOSEPH³

¹Center for Turbulence and Flow Control Research, Institute of Advanced Machinery and Design,
Seoul National University, Seoul 151-742, Korea

²School of Mechanical and Aerospace Engineering, Seoul National University,
Seoul 151-742, Korea

³Department of Aerospace Engineering and Mechanics, University of Minnesota,
107 Akerman Hall, 110 Union Street SE, Minneapolis, MN 55455, USA

(Received 15 March 2002 and in revised form 13 January 2003)

Turbulent drag reduction by polymer additives in a channel is investigated using direct numerical simulation. The dilute polymer solution is expressed with an Oldroyd-B model that shows a linear elastic behaviour. Simulations are carried out by changing the Weissenberg number at the Reynolds numbers of 4000 and 20 000 based on the bulk velocity and channel height. The onset criterion for drag reduction predicted in the present study shows a good agreement with previous theoretical and experimental studies. In addition, the flow statistics such as the r.m.s. velocity fluctuations are also in good agreement with previous experimental observations. The onset mechanism of drag reduction is interpreted based on elastic theory, which is one of the most plausible hypotheses suggested in the past. The transport equations for the kinetic and elastic energy are derived for the first time. It is observed that the polymer stores the elastic energy from the flow very near the wall and then releases it there when the relaxation time is short, showing no drag reduction. However, when the relaxation time is long enough, the elastic energy stored in the very near-wall region is transported to and released in the buffer and log layers, showing a significant amount of drag reduction.

1. Introduction

Since Toms (1949) reported turbulent drag reduction by polymer additives, there have been many studies on this phenomenon, including theoretical, experimental and numerical approaches. The two most important findings from experimental studies by Virk *et al.* (1967) and Virk (1971) are the onset of drag reduction and the existence of maximum drag reduction (MDR), suggesting that drag reduction does not come from a purely viscous effect of the dilute polymer solution (de Gennes 1990). That is, if the viscosity were a dominant parameter for drag reduction, the drag would decrease regardless of the amount of polymer concentration. However, experimental studies have shown the existence of a threshold concentration for drag reduction.

The first theoretical hypothesis about the onset of drag reduction is the ‘time criterion’ (Tulin 1966; Hershey & Zakin 1967; Lumley 1969). The time criterion indicates that drag reduction occurs when the relaxation time is longer than the time

scale of the near-wall turbulence, i.e.

$$\lambda > \frac{\nu}{u_\tau^2}, \quad (1.1)$$

where λ is the relaxation time, ν the kinematic viscosity of the solution, $u_\tau = \sqrt{\tau_w/\rho}$ the wall shear velocity, τ_w the wall shear stress, and ρ the density of the solution. The time criterion (1.1) was verified in the experiment of Berman (1977). Lumley (1973) explained that drag reduction comes from the elongational viscosity which is increased greatly by the ‘coil–stretch’ transition under the condition of (1.1). Hinch (1977) showed theoretically that the ‘coil–stretch’ transition results in a great increase in the elongational viscosity. However, the scenario of the elongational viscosity was criticized in that the ‘coil–stretch’ does not occur in turbulent flow with randomly fluctuating strain rates (de Gennes 1990; Smith & Chu 1998; Sreenivasan & White 2000).

On the other hand, Goldshtik, Zametalin & Shtern (1982) applied a perturbation method to viscoelastic models (Maxwell and Oldroyd-B models) and showed that drag reduction occurs when

$$We_\tau = \frac{\lambda u_\tau^2}{\nu} > \alpha, \quad (1.2)$$

where We_τ is the Weissenberg number normalized by u_τ and ν , and α depends on the viscoelastic model. Here, (1.2) is a similar expression to (1.1). However, it should be noted that (1.2) does not come from the concept of the elongational viscosity but from the concept of the elasticity. Goldshtik *et al.* suggested that the time criterion may come from the elastic effect of dilute polymer solution.

Some experimental studies (for example, Gyr & Tsinober 1997; den Toonder *et al.* 1997; Warholic, Massah & Hanratty 1999) reported the existence of a ‘stress deficit’ in drag-reducing flow, i.e.

$$T_{12} > \mu \frac{d\bar{u}}{dy} - \rho \overline{u'v'}, \quad (1.3)$$

where T_{12} is the total shear stress ($= \mu d\bar{u}/dy - \rho \overline{u'v'} + \tau_p$), μ the viscosity of the solution, \bar{u} the mean streamwise velocity, $-\rho \overline{u'v'}$ the Reynolds shear stress, and τ_p the time-averaged stress deficit. This suggests that the viscoelasticity should be the most important property of a dilute polymer solution for drag reduction because the elongational-viscosity hypothesis cannot show the existence of the stress deficit (den Toonder *et al.* 1997).

Meanwhile, de Gennes (1990) suggested an elastic theory for drag reduction that was elaborated by Sreenivasan & White (2000), in which the polymer molecules absorb the small-scale turbulence energy into the elastic energy and prohibit the turbulence cascade, resulting in drag reduction. Because the elastic theory was not concerned with the wall region, de Gennes (1990) suggested that drag reduction might occur before polymer molecules, injected into the core of the pipe or channel flow, reached the wall. However, an experiment by Cadot, Bonn & Douady (1998) has shown that the wall effect is important for polymer drag reduction.

Joseph (1990) also noted that elasticity plays a predominant role in drag reduction. He suggested that polymers always attenuate turbulence at small scales, and thus there should exist a natural cut-off scale provided by the shear wave speed u_c . Therefore, he

suggested a criterion for drag reduction such as (see Joseph & Christodoulou 1993)

$$u_\tau > u_c = \sqrt{\frac{\nu}{\lambda}}. \quad (1.4)$$

Note that (1.4) is of the same form as (1.1) and (1.2). Because the shear velocity u_τ is associated with the near-wall turbulence, Joseph's hypothesis on the elasticity can be linked with the wall turbulence.

Recently, direct numerical simulations (DNS) (Orlandi 1995; den Toonder *et al.* 1997; Sureshkumar, Beris & Handler 1997; Dimitropoulos, Sureshkumar & Beris 1998) have provided more information about polymer drag reduction. Orlandi (1995) and den Toonder *et al.* (1997) adopted elongational-viscosity models and obtained drag reduction. However, such models are based on inelastic constitutive equations, and thus cannot predict the onset of drag reduction and the 'stress deficit'. More recently, Sureshkumar *et al.* (1997) and Dimitropoulos *et al.* (1998) adopted viscoelastic models (finitely extensible, nonlinear elastic (FENE-P) and Giesekus models) and used an artificial diffusion scheme (AD) for the spatial discretization of the convection term in their constitutive equations. However, this scheme smears out the steep gradients of polymer stresses, resulting in less drag reduction. Therefore they had to introduce a larger elasticity to obtain an appropriate amount of drag reduction (see Min, Yoo & Choi 2001). In addition, none of those studies explained how the elasticity causes drag reduction.

The objective of the present study is to propose a mechanism responsible for drag reduction by polymer additives using DNS of turbulent flow in a channel. An Oldroyd-B model (linear Hookean dumbbells) is used to represent the behaviour of the polymer. The Reynolds numbers used in the previous studies using DNS are too small compared with those used in the experimental studies (Gyr & Tsinober 1997; Sreenivasan & White 2000). Therefore, in the present study, simulations are conducted for $Re_b = U_b h / \nu = 4000$ (the same order of magnitude as previous DNS studies) and $Re_b = 20000$ (the same order of magnitude as previous experimental studies) based on the bulk velocity U_b and channel height h . The results are compared with the previous experimental studies. Moreover, the transport equations for the kinetic and elastic energy are derived for the first time by using the 'elastic theory' of Tabor & de Gennes (1986). Energy transfer between the flow and the polymer is examined through the kinetic and elastic energy transport equations, from which the mechanism for drag reduction is elucidated.

2. Governing equations and numerical method

The non-dimensional governing equations of unsteady incompressible viscoelastic flow with an Oldroyd-B model are as follows:

$$\frac{\partial u_i}{\partial t} + \frac{\partial}{\partial x_j} (u_i u_j) = -\frac{\partial p}{\partial x_i} + \frac{\beta}{Re} \frac{\partial^2 u_i}{\partial x_j \partial x_j} + \frac{1 - \beta}{Re} \frac{\partial \tau_{ij}}{\partial x_j}, \quad (2.1)$$

$$\frac{\partial u_i}{\partial x_i} = 0, \quad (2.2)$$

$$\tau_{ij} + We \left(\frac{\partial \tau_{ij}}{\partial t} + u_m \frac{\partial \tau_{ij}}{\partial x_m} - \frac{\partial u_i}{\partial x_m} \tau_{mj} - \frac{\partial u_j}{\partial x_m} \tau_{mi} \right) = \frac{\partial u_i}{\partial x_j} + \frac{\partial u_j}{\partial x_i}, \quad (2.3)$$

where u_i is the velocity, p the pressure, τ_{ij} the polymer stress, $Re (= U\delta/\nu)$ the

Reynolds number, $We (= \lambda U/\delta)$ the Weissenberg number, U the centreline velocity of the fully developed laminar flow ($U = \frac{3}{2}U_b$), δ the channel half-height ($\delta = \frac{1}{2}h$), and β the ratio of solvent viscosity to the total viscosity of solution. In the present study, β is fixed at 0.9 for the case of a viscoelastic fluid, because the dilute solutions that give rise to drag reduction are nearly Newtonian in the sense that they have essentially the same viscosity as the solvent. For $Re = 3000$ ($Re_b = U_b h/\nu = 4000$; $Re_\tau = u_{\tau_0} \delta/\nu \simeq 135$), a calculation domain of $7\delta \times 2\delta \times 3.5\delta$ is chosen in the streamwise (x), wall-normal (y) and spanwise (z) directions, respectively, with a $64 \times 97 \times 96$ grid ($\Delta x^+ \simeq 15$, $\Delta y_{min}^+ \simeq 0.3$, $\Delta z^+ \simeq 5$). Here u_{τ_0} is the wall shear velocity for Newtonian fluid flow ($\beta = 1$). For $Re = 15000$ ($Re_b = 20000$; $Re_\tau \simeq 530$), the minimal channel concept by Jiménez & Moin (1991) is adopted† and a calculation domain of $2.4\delta \times 2\delta \times 0.9\delta$ is chosen with a $128 \times 257 \times 96$ grid ($\Delta x^+ \simeq 10$, $\Delta y_{min}^+ \simeq 0.4$, $\Delta z^+ \simeq 5$). The grid resolution used is almost the same as that of Moser, Kim & Mansour (1999). We impose the periodic boundary condition in the streamwise and spanwise directions, and the no-slip boundary condition in the wall-normal direction. A fully developed turbulent flow field of a Newtonian fluid ($\beta = 1$) is used as an initial condition for the simulation of viscoelastic fluid flow. A constant mass flow rate is maintained in the channel during simulation by adjusting the mean pressure gradient at each computational time step. In other words, the bulk Reynolds number (Re_b) is constant during a simulation.

The numerical algorithm is based on a semi-implicit, fractional-step method: the velocity diffusion and polymer stress derivative terms in (2.1) are advanced with the Crank–Nicolson method, and the velocity convection term in (2.1) and all the terms in (2.3) are advanced with a third-order Runge–Kutta method. A fourth-order compact difference scheme (COM4; Lele 1992) is used for the polymer-stress derivative $\partial\tau_{ij}/\partial x_j$ in (2.1), and a modified compact upwind difference scheme (MCUD3; Min *et al.* 2001) is used for the polymer-stress convection term $u_m \partial\tau_{ij}/\partial x_m$ in (2.3). All other terms are discretized using the second-order central difference (CD) scheme. Here, we briefly introduce COM4 and MCUD3 (for the detailed features of the present numerical method, see Min *et al.* 2001).

The spatial derivative of τ_{ij} in (2.1) is obtained using COM4, e.g.

$$\frac{\partial\tau_{ij}}{\partial x} \Big|^{q+1} + 4 \frac{\partial\tau_{ij}}{\partial x} \Big|^q + \frac{\partial\tau_{ij}}{\partial x} \Big|^{q-1} = \frac{3}{\Delta} (\tau_{ij}^{q+1} - \tau_{ij}^{q-1}) + O(\Delta^4), \quad (2.4)$$

where q is the index of a grid cell and Δ is the grid spacing. Equation (2.4) results in a tridiagonal matrix system, so one can easily obtain fourth-order accuracy for $\partial\tau_{ij}/\partial x$. The spatial derivative of τ_{ij} in (2.3) is obtained using a third-order compact upwind difference scheme (CUD3, Tolstykh & Lipavskii 1998), e.g.

$$\begin{aligned} & (2 - 3s^{q+1/2}) \frac{\partial\tau_{ij}}{\partial x} \Big|^{q+1} + (8 - 3s^{q+1/2} + 3s^{q-1/2}) \frac{\partial\tau_{ij}}{\partial x} \Big|^q + (2 + 3s^{q-1/2}) \frac{\partial\tau_{ij}}{\partial x} \Big|^{q-1} \\ & = \frac{6}{\Delta} [(1 - s^{q+1/2})\tau_{ij}^{q+1} + (s^{q+1/2} + s^{q-1/2})\tau_{ij}^q - (1 + s^{q-1/2})\tau_{ij}^{q-1}] + O(\Delta^3), \quad (2.5) \end{aligned}$$

† For larger Weissenberg numbers leading to near maximum drag reduction (MDR), this minimal channel concept is no longer valid because the turbulence structures become very large at the MDR state (Min, Choi & Yoo 2002).

where $s^{q+1/2}$ is the sign of the x -component velocity (u) between the q th and $(q+1)$ th cells, that is, $s^{q+1/2} = 1$ when $u^{q+1/2} \geq 0$, and $s^{q+1/2} = -1$ when $u^{q+1/2} < 0$. Here in CUD3, an upwinding is introduced to COM4 in order to have a dissipative error. When $s = 0$, CUD3 is equal to COM4.

It is known that the configuration tensor c_{ij} ($= We \tau_{ij} + \delta_{ij}$) loses its positive definiteness due to the accumulation of numerical errors, which results in numerical breakdown (Joseph 1990; Min *et al.* 2001). Thus, in MCUD3, we add a second-order artificial diffusion scheme (AD) to CUD3 at each time step at the locations where the determinant of the configuration tensor becomes negative, in order to prevent the numerical instability at an initial stage. The effect of the dissipative error caused by this AD on the flow field is negligible because the grid locations where AD is added change in time and the number of corresponding grid points is very small (at most less than 0.5%) for the present flow. Recently, MCUD3 was successfully utilized in Dubief & Lele (2001).

One might wonder if the resolution required for the simulation of viscoelastic fluid flow should be higher than that for the simulation of Newtonian fluid flow. In our study, we confirmed from simulations that for the present flow the polymeric stress derivatives in (2.1), $((1 - \beta)/Re)(\partial \tau_{ij}/\partial x_j)$, are the same order of magnitude as the Newtonian stress derivatives, $(\beta/Re)(\partial^2 u_i/\partial x_j \partial x_j)$. Thus, with the same resolution used for the Newtonian fluid flow, the use of COM4 for the polymeric stress derivatives in (2.1) and that of MCUD3 for the polymer-stress convection term in (2.3) should resolve the spatial distribution of the polymeric stresses. Furthermore, as we will show in the next section, our simulation results agree very well with the previous experimental results for the present flow, and the power spectra of the polymeric stresses do not show any power accumulation at high wavenumbers. Nevertheless, it should be noted that the present low-order schemes used for the spatial derivatives may require higher resolution to obtain high-order turbulence statistics (Choi, Moin & Kim 1992).

We have also separately simulated the same flow with a different viscoelastic model, FENE-P, to see how the unboundedness of the polymer stretch in the Oldroyd-B model affects the drag and velocity field. In the Appendix, we clearly show that the Oldroyd-B model does not produce any unbounded polymer stretch, at least for the present flow, and the drag and r.m.s. velocity fluctuations are nearly the same as those obtained from the FENE-P model (see the Appendix for the details).

3. Changes in the flow variables

3.1. Drag variation and onset criterion of drag reduction

Figure 1 shows the time histories of the mean pressure gradient that drives a constant mass flow rate in a channel at $Re = 3000$ and $15\,000$, normalized by that of Newtonian fluid flow $(-d\bar{p}/dx|_0)$. The percentage drag reduction (DR) is defined as

$$DR = \frac{(-d\bar{p}/dx|_0) - (-d\bar{p}/dx)}{-d\bar{p}/dx|_0} \times 100. \quad (3.1)$$

Table 1 shows the variation of the drag with the Weissenberg number. It is seen that drag reduction occurs at $We > 1$ and $We > 0.3$, respectively, for $Re = 3000$ and $15\,000$, and the drag decreases more with larger Weissenberg number. The drag neither decreases nor increases at $We = 0.1, 0.5$ and 1 for $Re = 3000$ and at $We = 0.2$ and 0.3 for $Re = 15\,000$, respectively. This indicates that there exists a threshold for the

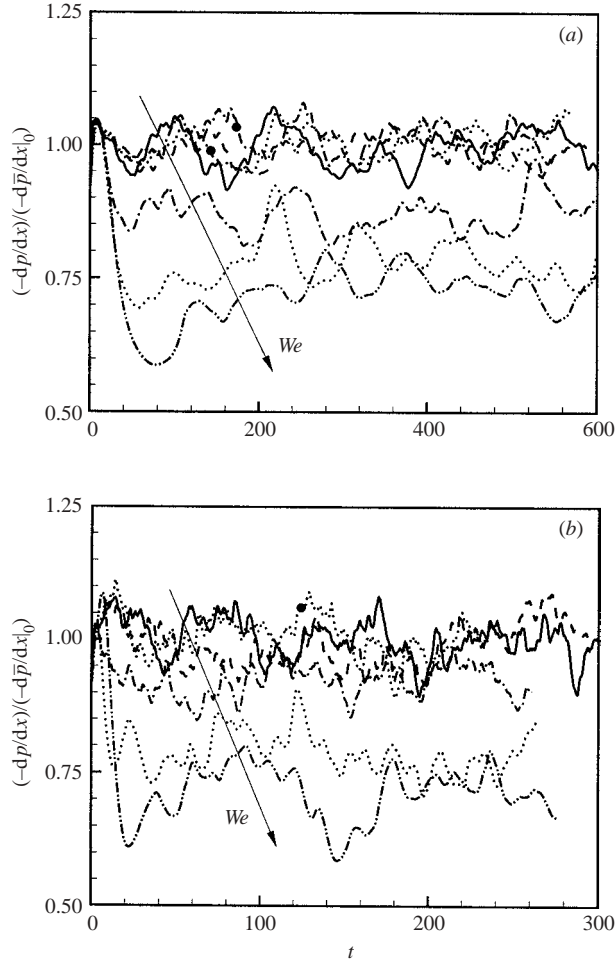


FIGURE 1. Time histories of the mean pressure gradient normalized by that of Newtonian fluid flow. (a) $Re = 3000$ (—, Newtonian; ·····, ●, $We = 0.1$; -·-·-, ●, $We = 0.5$; ---, $We = 1$; - - - - , $We = 2$; ·····, $We = 3$; -·-·-·-, $We = 4$). (b) $Re = 15000$ (—, Newtonian; ·····, ●, $We = 0.2$; ---, $We = 0.3$; -·-·-·-, $We = 0.5$; ·····, $We = 1$; -·-·-·-, $We = 2$).

Weissenberg number to achieve drag reduction. The onset Weissenberg number We_τ normalized by u_{τ_0} and ν for drag reduction is about 6 for both Reynolds numbers.

The ‘time criterion’ suggested by Lumley (1969) indicated that the onset We_τ for drag reduction is 1. Berman (1977) showed that the onset We_τ ranges from 1 to 8 depending on the properties of polymers and solvents. Goldshtik *et al.* (1982) studied the polymer drag reduction theoretically and suggested that the onset We_τ is 1 for the Maxwell model and $5 \sim 6$ for the Oldroyd-B model with $\beta = 0.9$.

Orlandi (1995) and den Toonder *et al.* (1997) could not predict the onset We_τ from their direct numerical simulations because they used inelastic constitutive models. Sureshkumar *et al.* (1997) and Dimitropoulos *et al.* (1998) showed that drag reduction occurred at $We_\tau = 25$ but not at $We_\tau = 12.5$. This Weissenberg number is much larger than the onset Weissenberg number obtained from experimental and theoretical studies. As mentioned previously, the numerical schemes used in Sureshkumar *et al.* (1997) and Dimitropoulos *et al.* (1998) smear out the steep gradient of polymer

Re^\dagger	We^\ddagger	We_τ	DR (%)
3000	0.1	0.60	0
	0.5	3.0	0
	1	6.0	0
	2	12	12
	3	18	20
	4	24	27
15 000	0.2	3.7	0
	0.3	5.6	0
	0.5	9.3	8
	1	19	21
	2	37	28
	$\dagger Re_b = U_b h / \nu = \frac{4}{3} Re.$		
	$\ddagger We_b = \lambda U_b / h = \frac{1}{3} We.$		

TABLE 1. Variation of the drag with respect to the Weissenberg number at $Re = 3000$ and $15\,000$.

stresses, which may result in less or no drag reduction at a Weissenberg number larger than the threshold value (see also Min *et al.* 2001). On the other hand, the onset Weissenberg number obtained from the present study shows excellent agreement with previous theoretical and experimental results.

3.2. Mean velocity and turbulence intensities

The mean velocity profiles normalized by the wall-shear velocity u_τ are shown in figure 2, together with the experimental results by Luchik & Tiederman (1988) and Wei & Willmarth (1992). Here, $u^+ = \bar{u}/u_\tau$, $y^+ = yu_\tau/\nu$, and \bar{u} is the mean streamwise velocity. It is difficult to compare numerical results with experimental ones, because the parameters in the constitutive equations are not easy to obtain from the polymer used in the experiments (Joseph 1990). However, the experimental studies in Luchik & Tiederman (1988) and Wei & Willmarth (1992) were conducted at the Reynolds numbers of $Re_\tau \simeq 520$ and 570 , respectively, which are very similar to that of the present study ($Re_\tau \simeq 530$). Furthermore, the amounts of drag reduction reported in Luchik & Tiederman (1988) and Wei & Willmarth (1992) are, respectively, 20% and 30%, which are also nearly identical to those obtained in the present study (21% and 28% for $We = 1$ and 2 , respectively). Therefore, the results from two experimental studies are compared with the present ones in figure 2(b).

It is evident from figure 2 that the mean velocity profiles agree very well with the experimental results. Also, upward shifts in the log-law are clearly observed for the drag-reducing flows, which has been observed in other types of drag-reducing flows such as flow over riblets (Choi, Moin & Kim 1993) and flow with active blowing and suction (Choi, Moin & Kim 1994). It is also noticeable on figure 2 that the viscous sublayer thickness increases for the drag-reducing flows (we also confirmed this finding from the plot of u^+/y^+ vs. y^+), which has been previously observed in the experimental studies (Luchik & Tiederman 1988; Wei & Willmarth 1992). Goldshtik *et al.* (1982) reported that the viscous sublayer thickness does not change for the Maxwell model ($\beta = 0$) and the Oldroyd-B model with a short retardation time such as $\beta = 0.2$, but it increases for the Oldroyd-B model with a long

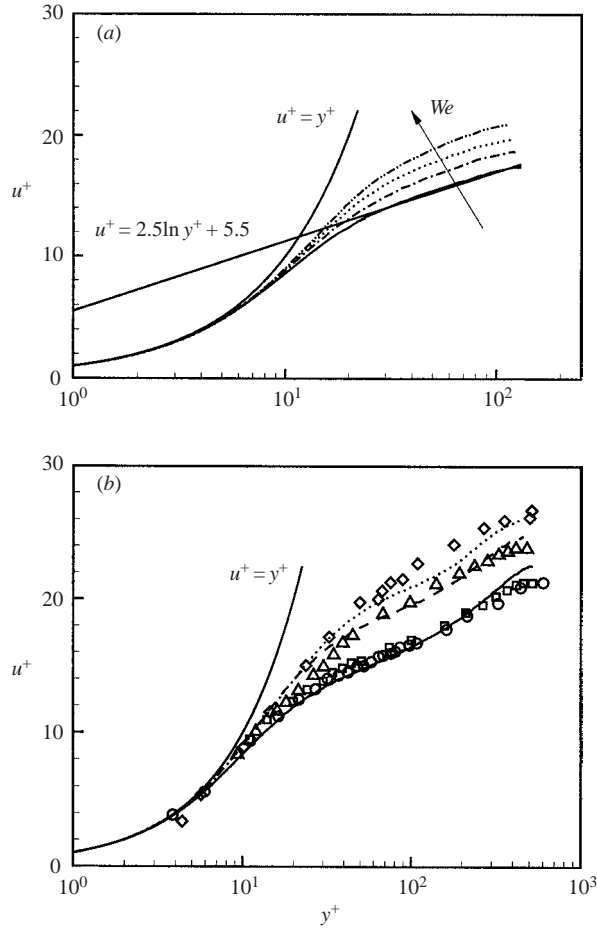


FIGURE 2. Mean streamwise velocities normalized by the wall-shear velocity u_τ . (a) $Re = 3000$ (—, Newtonian; ---, $We = 1$; -.-.-, $We = 2$; , $We = 3$; -.-.-.-, $We = 4$). (b) $Re = 15000$ (—, Newtonian; ---, $We = 1$; , $We = 2$). Also shown are the experimental results from Luchik & Tiederman (1988: \square , Newtonian; \triangle , polymer) and Wei & Willmarth (1992: \circ , Newtonian; \diamond , polymer).

retardation time such as $\beta = 0.9$ and 0.95 . Therefore, the increase in the viscous sublayer thickness from the present study also shows good agreement with the theory of Goldshtik *et al.* (1982) because $\beta = 0.9$ for the present study.

The variation of the root-mean-square (r.m.s.) velocity fluctuations with the Weissenberg number is shown in figure 3, together with the experimental results by Luchik & Tiederman (1988) and Wei & Willmarth (1992). As the Weissenberg number increases, the r.m.s. streamwise velocity fluctuations decrease very near the wall but increase away from the wall, whereas the r.m.s. wall-normal and spanwise velocity fluctuations decrease in the whole channel. It is seen that the present results are also in good agreement with the experimental results of Luchik & Tiederman (1988) and Wei & Willmarth (1992). The increase in u_{rms} in a drag-reducing flow was also observed in a turbulent channel flow with a streamwise magnetic field (Lee & Choi 2001), whereas the decrease in u_{rms} was observed in flow above riblets (Choi *et al.* 1993) and flow with active blowing and suction (Choi *et al.* 1994), indicating that the

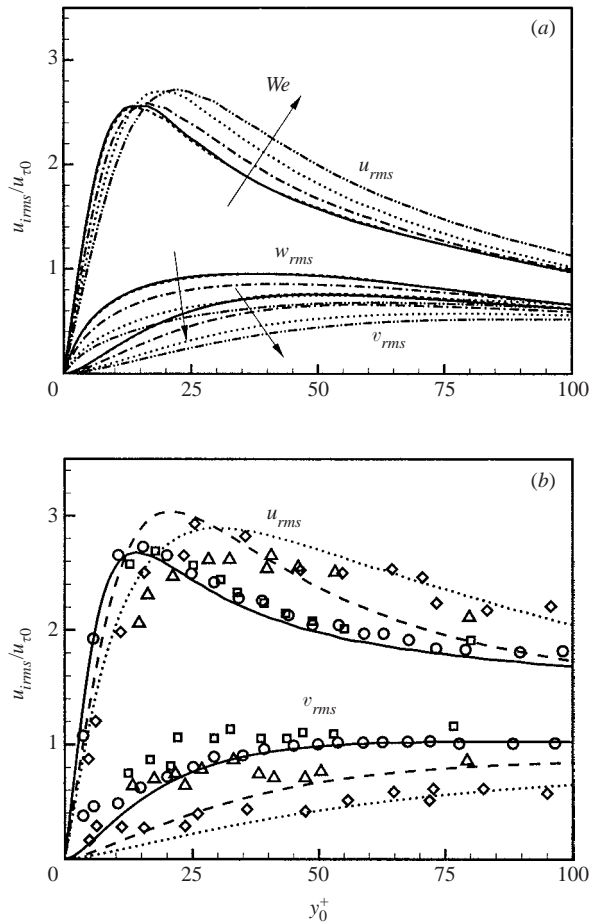


FIGURE 3. Root-mean-square velocity fluctuations normalized by the wall-shear velocity u_{τ_0} : (a) $Re = 3000$; (b) $Re = 15000$. Lines and symbols are the same as those in figure 2. Here, $y_0^+ = yu_{\tau_0}/\nu$.

variation of u_{rms} is not a direct indication of drag reduction. Warholic *et al.* (1999) also reported a decrease in u_{rms} in the case of large drag reduction for turbulent polymer flow, while u_{rms} increases in the case of small drag reduction. On the other hand, the r.m.s. cross-velocity fluctuations decreased for all the drag-reducing flows. The turbulent kinetic energy showed the same trend as the r.m.s. streamwise velocity fluctuations (not shown here), because u_{rms} is much larger than v_{rms} and w_{rms} .

The variation of the r.m.s. vorticity fluctuations with the Weissenberg number is shown in figure 4. All three components of the vorticity fluctuations substantially decrease with increasing Weissenberg number. It is also noticeable that the y -location of the local maximum of the streamwise vorticity fluctuations moves further away from the wall with increasing Weissenberg number, which indicates that the streamwise-vortex centre moves away from the wall in the turbulent flow of polymeric liquids and the sweep motion induced by those streamwise vortices is less effective in producing a high skin friction.

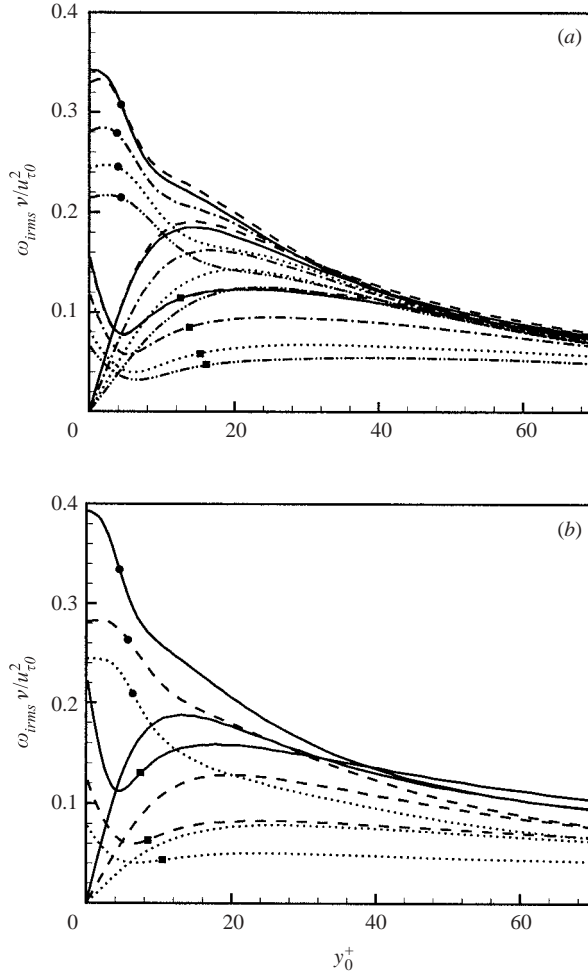


FIGURE 4. Root-mean-square vorticity fluctuations normalized by the wall-shear velocity u_{τ_0} : (a) $Re = 3000$; (b) $Re = 15000$. Lines are the same as those in figure 2. Lines with \blacksquare denote ω_x , unadorned lines ω_y and lines with \bullet ω_z , respectively.

3.3. Reynolds shear stress and stress deficit

The Reynolds shear stress, $-\rho \overline{u'v'}$, and total shear stress, $T_{12} = \mu d\bar{u}/dy - \rho \overline{u'v'} + \tau_p$, normalized by u_{τ_0} are shown in figure 5, together with the Reynolds shear stress from the experimental studies by Luchik & Tiederman (1988) and Wei & Willmarth (1992). The total shear stress should be a straight line when the flow reaches a fully developed state, and the present result shows that this is indeed the case. The slope of the total shear stress decreases with increasing Weissenberg number, because the mean pressure gradient required to drive a constant mass flux in a channel decreases (see figure 1). A significant reduction in the Reynolds shear stress is also observed throughout the channel with the polymer additives. It is seen that the present results for $-\overline{u'v'}$ are in good agreement with the experimental results of Luchik & Tiederman (1988). Note that the disagreement with the polymer case of Wei & Willmarth (1992) might come from a mistake in their data implementation since the slope of their Reynolds shear stress in the channel centre suggests much larger drag reduction (about 50%) than what they actually obtained (30%).

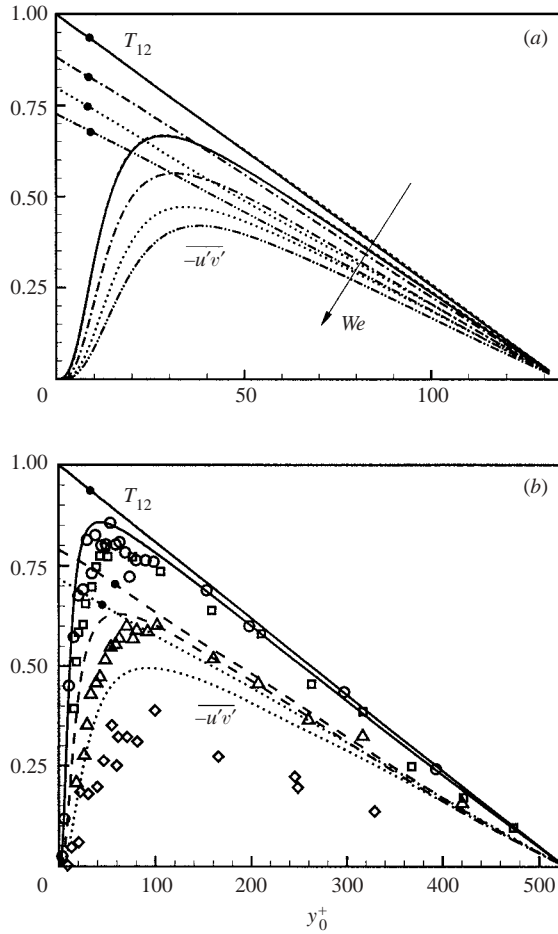


FIGURE 5. Reynolds shear stresses and total shear stresses normalized by the wall-shear velocity u_{τ_0} : (a) $Re = 3000$; (b) $Re = 15000$. Lines and symbols for the Reynolds shear stress are the same as those in figure 2. Lines with \bullet denote the total shear stress.

One of the most interesting features in turbulent drag reduction of a dilute polymer solution is the ‘stress deficit’, which was already defined in (1.3). For an Oldroyd-B model, (1.3) can be derived as

$$\begin{aligned}
 T_{12} &= \mu_N \frac{d\bar{u}}{dy} - \rho \overline{u'v'} + \bar{\tau}_{12} \\
 &= \mu_N \frac{d\bar{u}}{dy} - \rho \overline{u'v'} + \mu_E \frac{d\bar{u}}{dy} + \tau_p \\
 &= \mu \frac{d\bar{u}}{dy} - \rho \overline{u'v'} + \tau_p,
 \end{aligned}
 \tag{3.2}$$

where μ_N is the Newtonian viscosity and μ_E the elastic viscosity. The Newtonian viscosity μ_N is not the solvent viscosity μ_s but is interpreted as an effective Newtonian contribution to the solution viscosity μ (see Joseph 1990, Chap. 18). It is not easy to measure the correct values of μ_N , whereas μ and μ_s can be also easily measured using a viscometer. Since we consider a dilute polymer solution where μ is almost

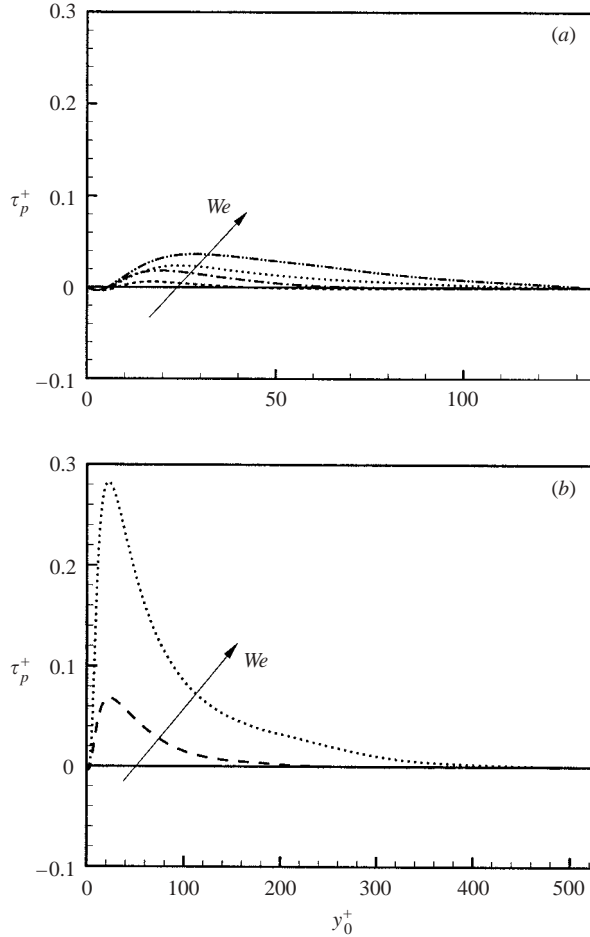


FIGURE 6. Stress deficits normalized by the wall-shear velocity u_τ : (a) $Re = 3000$; (b) $Re = 15000$. Lines are the same as those in figure 2.

the same as μ_s , (3.2) can be also expressed as (see also Warholic *et al.* 1999)

$$T_{12} = \mu_s \frac{d\bar{u}}{dy} - \overline{\rho u'v'} + \tau_p. \quad (3.3)$$

The total shear stress normalized by the wall-shear velocity u_τ is

$$T_{12}^+ = \frac{du^+}{dy^+} - \overline{u'^+v'^+} + \tau_p^+, \quad (3.4)$$

where τ_p^+ is the dimensionless stress deficit caused by polymer additives that cannot be predicted by an inelastic theory although it is observed experimentally (see den Toonder *et al.* 1997). Figure 6 shows the stress deficit obtained from the present study. The stress deficit increases with increasing Weissenberg number, and its maximum is in the buffer layer, which was also reported in the experimental result by den Toonder *et al.* (1997). Note also that τ_p becomes large with increasing Reynolds number.

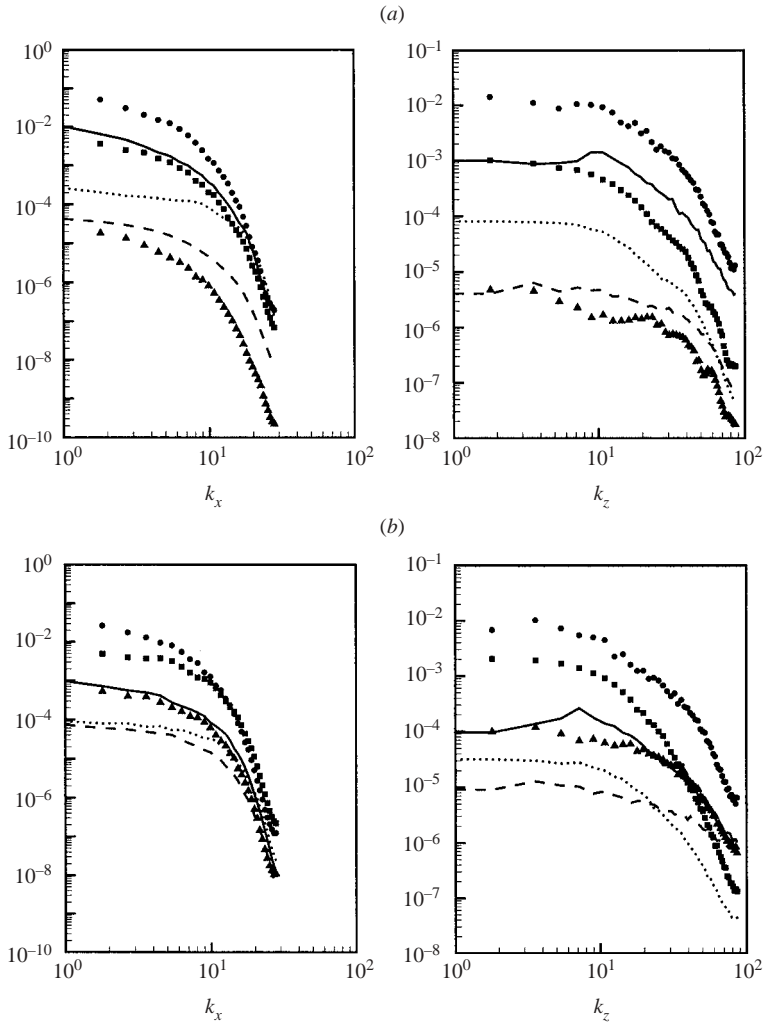


FIGURE 7. Power spectra of the polymer stresses normalized by $u_{\tau_0}^2$ at $Re = 3000$: (a) $y_0^+ \simeq 10$; (b) $y_0^+ \simeq 30$. For $We = 1$ (no drag reduction): —, $((1 - \beta)/Re)\tau_{11}$; ---, $((1 - \beta)/Re)\tau_{22}$; ·····, $((1 - \beta)/Re)\tau_{33}$; for $We = 3$ (20% drag reduction): ●, $((1 - \beta)/Re)\tau_{11}$; ▲, $((1 - \beta)/Re)\tau_{22}$; ■, $((1 - \beta)/Re)\tau_{33}$.

3.4. Power spectra of the polymer stresses τ_{11} , τ_{22} and τ_{33}

Figure 7 shows the power spectra of the polymer stresses, $((1 - \beta)/Re)\tau_{11}$, $((1 - \beta)/Re)\tau_{22}$ and $((1 - \beta)/Re)\tau_{33}$, at $Re = 3000$ for the cases of no drag reduction and 20% drag reduction. Here k_x and k_z are the streamwise and spanwise wavenumbers, respectively. The power spectra shown in this figure illustrate that the present grid resolution is adequate, because the power density at high wavenumbers is a few to several decades lower than that at low wavenumbers, and there is no evidence of power accumulation at high wavenumbers. At $y_0^+ \simeq 30$, all the polymer stresses increase with increasing Weissenberg number irrespective of drag reduction. However, at $y_0^+ \simeq 10$ (near the wall), τ_{11} and τ_{33} increase but τ_{22} decreases when drag reduction occurs. This phenomenon is in good agreement with the near-wall analysis of Goldshtik *et al.* (1982): the stretching stresses acting in the near-wall plane parallel to the wall (τ_{11}

and τ_{33}) may damp out the near-wall wall-normal motion. These different behaviours of the polymer stretch at different wall-normal locations are closely associated with the present drag reduction mechanism, which will be presented in the next section.

4. Drag-reduction mechanism

The elastic theory was first suggested by Tabor & de Gennes (1986). They assumed that polymers in solvent behave like an elastic spring. When the spring is a linear one, the elastic energy per unit volume stored by polymers can be expressed as

$$k_p^* = \frac{1}{2}nG(\langle Q^2 \rangle - \langle Q^2 \rangle_{eq}), \quad (4.1)$$

where n is the number of polymer molecules per unit volume, G the elastic modulus, $\langle Q^2 \rangle$ the ensemble average of polymer length squared, and the subscript 'eq' denotes the equilibrium state. However, when the spring is not a linear one, expression (4.1) should be modified. For example, Pincus (1976) reported that the elastic energy is proportional to $\langle Q^{5/4} \rangle$ rather than $\langle Q^2 \rangle$ (see also de Gennes 1990 and Sreenivasan & White 2000). Since the polymer molecule in the Oldroyd-B model is regarded as a linear dumbbell, the nonlinear elastic effect is neglected in the framework of the present approach.

From the kinetic theory (Bird *et al.* 1987, p. 72), $\langle Q^2 \rangle$ and $\langle Q^2 \rangle_{eq}$ can be derived as follows:

$$\left. \begin{aligned} \langle Q^2 \rangle &= \frac{3k_B T}{G} + \frac{\tau_{ii}^*}{nG}, \\ \langle Q^2 \rangle_{eq} &= \frac{3k_B T}{G}, \end{aligned} \right\} \quad (4.2)$$

where k_B is the Boltzmann constant, T is the absolute temperature, and τ_{ii}^* is the trace of the dimensional polymer stress. Then, k_p^* becomes

$$k_p^* = \frac{1}{2}\tau_{ii}^*, \quad (4.3)$$

or in a non-dimensional form,

$$k_p = \frac{1}{2} \frac{1 - \beta}{Re} \tau_{ii}. \quad (4.4)$$

Using the definition of the elastic energy k_p in (4.4), one can obtain the transport equations for the kinetic and elastic energy from the momentum and constitutive equations as follows:

$$\left\langle \frac{Dk_m}{Dt} \right\rangle = -\langle P_k \rangle - \langle P_{e,m} \rangle + \langle P_w \rangle + \beta \left\langle \frac{1}{Re} \frac{d^2 k_m}{dy^2} \right\rangle - \beta \langle \epsilon_m \rangle, \quad (4.5)$$

$$\left\langle \frac{Dk_t}{Dt} \right\rangle = \langle P_k \rangle - \langle P_{e,t} \rangle + \beta \left\langle \frac{1}{Re} \frac{d^2 k_t}{dy^2} \right\rangle - \beta \langle \epsilon_k \rangle, \quad (4.6)$$

$$\left\langle \frac{Dk_e}{Dt} \right\rangle = \langle P_{e,m} \rangle + \langle P_{e,t} \rangle - \frac{1}{We} \langle k_e \rangle, \quad (4.7)$$

where

$$\begin{aligned}
 k_m &= \frac{1}{2}\bar{u}^2, & k_t &= \frac{1}{2}\overline{u'_i u'_i}, & k_e &= \bar{k}_p, \\
 P_k &= -\overline{u'v'} \frac{d\bar{u}}{dy}, & P_{e,m} &= \frac{1-\beta}{Re} \bar{\tau}_{12} \frac{d\bar{u}}{dy}, \\
 P_w &= -\bar{u} \frac{d\bar{p}}{dx}, & \epsilon_m &= \frac{1}{Re} \frac{d\bar{u}}{dy} \frac{d\bar{u}}{dy}, \\
 P_{e,t} &= \frac{1-\beta}{Re} \overline{\frac{\partial u'_i}{\partial x_j} \tau'_{ij}}, & \epsilon_k &= \frac{1}{Re} \overline{\frac{\partial u'_i}{\partial x_j} \frac{\partial u'_i}{\partial x_j}}.
 \end{aligned}$$

Here $\langle \cdot \rangle = (1/V) \int \cdot dV$ and V is the total volume of the computational domain. Equations (4.5)–(4.7) provide the information about the energy transfer between the polymer and the flow. The energy transfer between the mean kinetic energy k_m and the turbulent kinetic energy k_t is executed through P_k . The energy transfer between the mean kinetic energy k_m and the elastic energy k_e is through $P_{e,m}$, and that between the turbulent kinetic energy k_t and the elastic energy k_e is through $P_{e,t}$. The turbulent kinetic energy k_t is dissipated by ϵ_k and the elastic energy k_e dissipates itself.

Figure 8 shows the time histories of the volume-averaged production $\langle P_k \rangle$ and dissipation $\langle \epsilon_k \rangle$ of the turbulent kinetic energy. The mean values of $\langle P_k \rangle$ and $\langle \epsilon_k \rangle$ decrease with increasing We when drag reduction occurs, because turbulence inside the channel becomes weaker. However, it is interesting to note that the fluctuating amplitudes of $\langle P_k \rangle$ and $\langle \epsilon_k \rangle$ become larger as We increases. This phenomenon is associated with the temporal variation of the elastic energy, which will be discussed later. The spatial distributions of P_k and ϵ_k are shown in figure 9. The production and dissipation of the turbulent kinetic energy decrease throughout the channel with the polymer additives.

Figure 10 shows the time histories of the volume-averaged productions, $\langle P_{e,m} \rangle$ and $\langle P_{e,t} \rangle$, and dissipation, $-\langle k_e \rangle / We$, of the elastic energy. In the case of no drag reduction ($We = 1$ and 0.3 for $Re = 3000$ and 15000 , respectively), $\langle P_{e,m} \rangle$, $\langle P_{e,t} \rangle$ and $-\langle k_e \rangle / We$ are nearly constant in time, indicating that the energy transfer from the flow to the polymer is nearly steady and the amount of energy received from both the mean and turbulent kinetic energy is dissipated by the elastic energy itself (see (4.7)). Interestingly, as shown in figure 11, the values of $\langle P_{e,m} \rangle$, $\langle P_{e,t} \rangle$ and $-\langle k_e \rangle / We$ are nearly the same irrespective of We in the case of no drag reduction (i.e. in the case of $We \leq 1$ at $Re = 3000$). This means that the amount of energy transfer from the mean and turbulent kinetic energy to the elastic energy is the same irrespective of We in the case of no drag reduction, which again indicates that, with the polymer, $(1-\beta)$ times the dissipation and diffusion of the Newtonian fluid is replaced by $\langle P_{e,m} \rangle$ and $\langle P_{e,t} \rangle$, resulting in no change in the flow. That is, in the case of no drag reduction, the following relation should be valid:

$$\left. \begin{aligned}
 \langle P_{e,m} \rangle &= (1-\beta) \langle \epsilon_m \rangle_{\text{Newtonian}} - (1-\beta) \left\langle \frac{1}{Re} \frac{d^2 k_m}{dy^2} \right\rangle_{\text{Newtonian}}, \\
 \langle P_{e,t} \rangle &= (1-\beta) \langle \epsilon_k \rangle_{\text{Newtonian}} - (1-\beta) \left\langle \frac{1}{Re} \frac{d^2 k_t}{dy^2} \right\rangle_{\text{Newtonian}}.
 \end{aligned} \right\} \quad (4.8)$$

Then, substituting (4.8) into (4.5) and (4.6), one can clearly see that the dynamic equations for the mean and turbulent kinetic energy become the same as those for

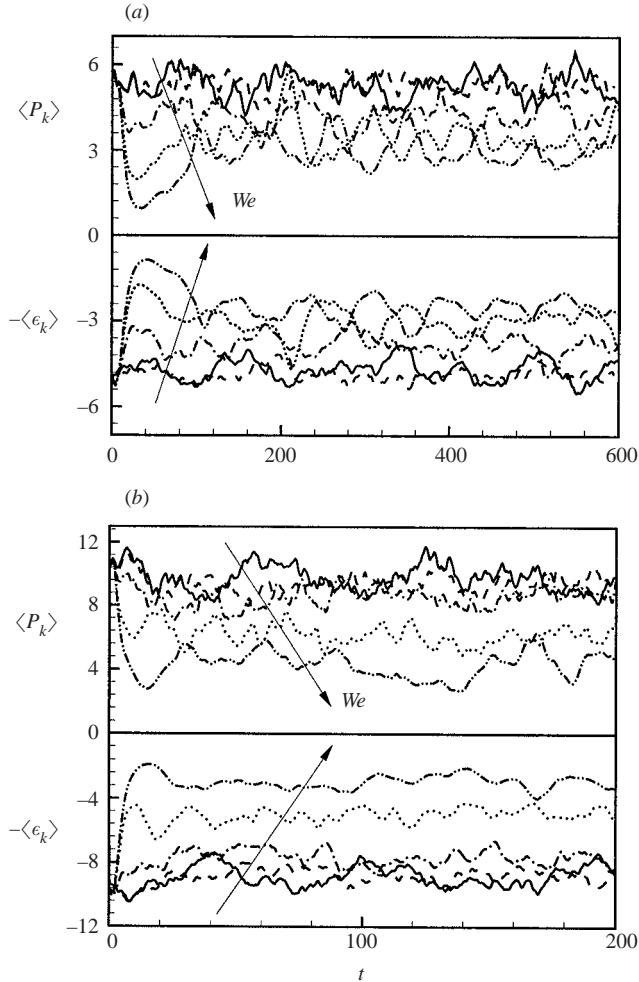


FIGURE 8. Time histories of the volume-averaged production $\langle P_k \rangle$ and dissipation $\langle \epsilon_k \rangle$ of the turbulent kinetic energy normalized by $u_{\tau 0}^3 / \delta$: (a) $Re = 3000$; (b) $Re = 15000$. The lines are the same as those in figure 1.

the Newtonian fluid flow. In figure 11, solid lines denote the magnitudes of $(1 - \beta)$ times the dissipations of the mean and turbulent kinetic energy, and their sum for the Newtonian fluid flow, which clearly shows the validity of (4.8) in the case of no drag reduction because the magnitude of the second term on the right-hand side of (4.8) is much smaller than that of the first term. However, when drag reduction occurs (for example, at $We = 3$ and 1 at $Re = 3000$ and 15000, respectively), the energy transfer becomes quite intermittent and more energy is transferred from the flow to the polymer, as shown in figure 10.

In order to investigate the detailed features of the energy transfer, the spatial distributions of $P_{e,m}$, $P_{e,t}$ and $-k_e / We$ are shown in figure 12. It is seen that the polymer stores and releases most energy near the wall. Although the amounts of the production and dissipation of elastic energy increase globally with increasing We (figure 10), they decrease locally very near the wall ($y^+ \leq 10$) but increase in the buffer and log layers. Interestingly, the same feature was observed for u_{rms} (figure 3) and the

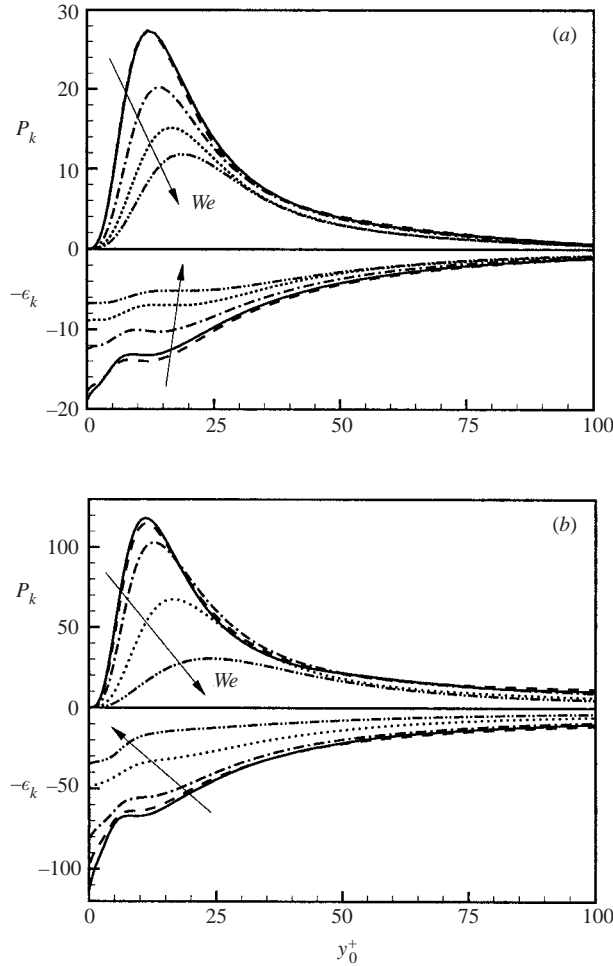


FIGURE 9. Profiles of the production P_k and dissipation ϵ_k of the turbulent kinetic energy normalized by $u_{\tau_0}^3/\delta$: (a) $Re = 3000$; (b) $Re = 15000$. The lines are the same as those in figure 1.

turbulent kinetic energy. Thus, we conjecture that, when drag reduction occurs, the polymer takes less energy from the flow in the very near-wall region and returns more energy to the flow in the buffer and log layers, and also that the polymer transports its elastic energy stored in the very near-wall region to the flow in the buffer and log layers.

This conjecture can be verified from the probability density function (PDF) of the elastic-energy production. The PDFs of $P_{e,m}$ and $P_{e,t}$ are shown in figure 13. Negative values of $P_{e,m}$ and $P_{e,t}$ represent the transport of the elastic energy of the polymer to the mean and turbulent kinetic energy of the flow, respectively. The probabilities of having negative $P_{e,m}$ and $P_{e,t}$ are shown in table 2. The energy transfer from the elastic energy to the mean kinetic energy (i.e. $P_{e,m} < 0$) at either $y_0^+ \simeq 5$ or 30 is nearly unchanged for different Weissenberg number. However, a significant change occurs in the energy transfer from the elastic energy to the turbulent kinetic energy (i.e. $P_{e,t} < 0$) at $y_0^+ \simeq 30$ when drag reduction occurs. That is, this energy transfer significantly increases at $y_0^+ \simeq 30$ (from 3% at $We = 1$ to 31% at $We = 3$), indicating that, in

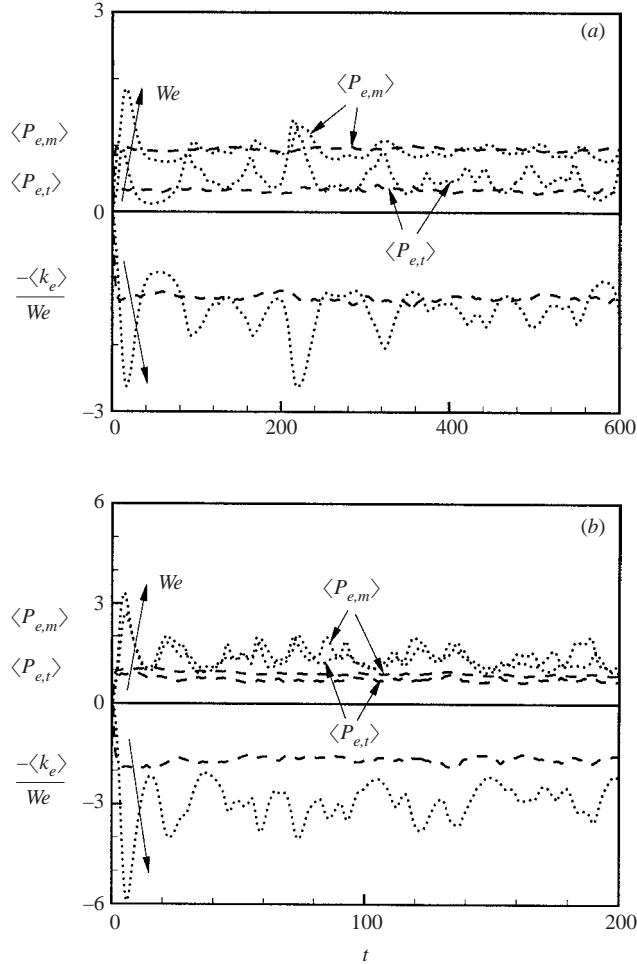


FIGURE 10. Time histories of the volume-averaged productions, $\langle P_{e,m} \rangle$ and $\langle P_{e,t} \rangle$, and dissipation, $-\langle k_e \rangle / We$, of the elastic energy normalized by $u_{\tau_0}^3 / \delta$: (a) $Re = 3000$ (---, $We = 1$; ·····, $We = 3$); (b) $Re = 15000$ (---, $We = 0.3$; ·····, $We = 1$).

the case of drag reduction, the polymer returns much more energy to the flow in the buffer layer than in the case of no drag reduction.

In order to see that the near-wall elastic energy is transported to the buffer and log layers, the time sequence of the elastic energy k_p in a coordinate system moving with the structures is shown in figure 14 for the cases with and without drag reduction at $Re = 3000$. In the case of no drag reduction ($We = 1$), high elastic energy exists only very near the wall. However, when drag reduction occurs ($We = 3$), high elastic energy existing very near the wall is transported to the buffer and log layers even though the cross-plane velocity fluctuations are much weaker than those for $We = 1$. A similar behaviour was also observed for $Re = 15000$.

The relaxation time of the polymer solution is essentially associated with the transport of the elastic energy. Fluid particles containing high elastic energy very near the wall are lifted away from the wall by the near-wall vortical motion (see figure 15). When the relaxation time is short (i.e. low We), the particles release the elastic

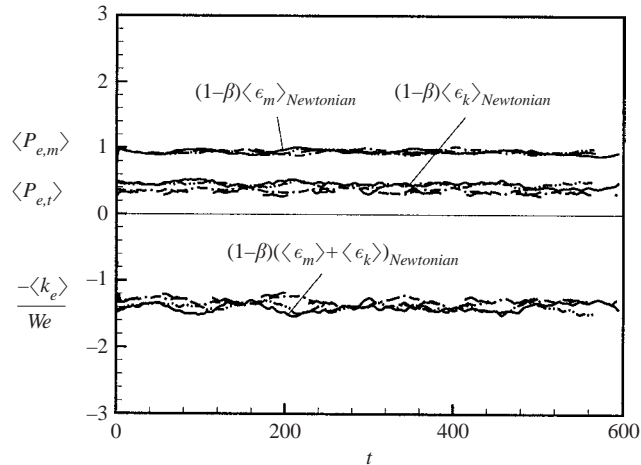


FIGURE 11. Time histories of the volume-averaged productions, $\langle P_{e,m} \rangle$ and $\langle P_{e,t} \rangle$, and dissipation, $-\langle k_e \rangle / We$, of the elastic energy normalized by $u_{\tau_0}^3 / \delta$ ($Re = 3000$): $-\cdots-$, $We = 0.1$; $-\cdot-\cdot-$, $We = 0.5$; $---$, $We = 1$. Solid lines in this figure denote the magnitudes of $(1 - \beta)$ times the dissipations of the mean and turbulent kinetic energy, and their sum for the Newtonian fluid flow.

energy very near the wall before they reach the buffer layer. When the relaxation time is long enough, however, the elastic energy absorbed from the kinetic energy is delivered to the buffer and log layers and released there, which results in weakening of near-wall turbulence (see also figure 3). Massah & Hanratty (1997) showed that the polymer chains are stretched in the very near-wall region (meaning that the polymer absorbs much elastic energy) and released in the buffer and log layers, supporting the present drag-reduction mechanism. The dynamic sequence in figure 15 also explains the intermittent energy transport behaviour shown in figure 10 in the case of drag reduction.

5. Conclusions and further remarks

In the present study, direct numerical simulation of turbulent viscoelastic flow in a channel was conducted to investigate the drag-reduction mechanism by polymer additives. An Oldroyd-B model was used for the constitutive equation for the polymer stress to represent the viscoelastic nature of the polymer. The simulations were carried out by changing the Weissenberg number at the bulk Reynolds numbers of 4000 and 20000.

The onset criterion for drag reduction predicted in the present study was in good agreement with previous theoretical and experimental studies. The flow statistics such as the mean velocity, turbulence intensities and Reynolds shear stress were also in good agreement with those in the previous experimental studies. In addition, the stress deficit that shows the role of the elasticity in drag reduction was observed.

The transport equations for the mean and turbulent kinetic energy and elastic energy were derived from the kinetic and elastic theory and were investigated. From the probability density functions of the production terms in those transport equations and also from the time sequence of the polymer elastic energy, we deduced the following mechanism for drag reduction by polymer additives. When drag reduction occurs, the turbulent kinetic energy near the wall is absorbed by the polymer and

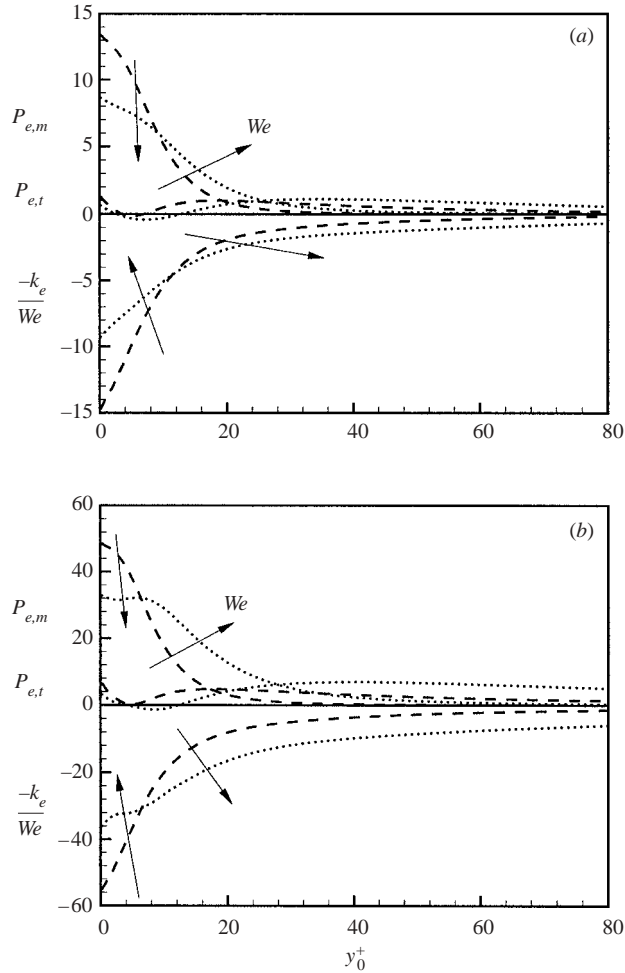


FIGURE 12. Profiles of the productions, $P_{e,m}$ and $P_{e,t}$, and dissipation, $-k_e/We$, of the elastic energy normalized by $u_{\tau_0}^3/\delta$: (a) $Re = 3000$ (---, $We = 1$; , $We = 3$); (b) $Re = 15000$ (---, $We = 0.3$; , $We = 1$).

transformed into elastic energy. Then, this elastic energy near the wall is lifted up by the near-wall vortical motion and released as turbulent kinetic energy or is dissipated in the buffer and log layers. Thus, the polymer actively intervenes in the energy transfer. Therefore, in order to obtain drag reduction, the relaxation time of the polymer should be long enough to transport the elastic energy from the near-wall region to the buffer or log layer. Otherwise, the elastic energy obtained near the wall is released there and an equilibrium state exists in terms of energy exchange, resulting in no drag change.

The drag-reduction mechanism proposed here in terms of the elastic theory does not imply that the mechanism based on the extensional viscosity is incorrect, as Sreenivasan & White (2000) mentioned. This is because any reasonable viscoelastic model (such as the FENE-P model or the Oldroyd-B model) suggests that an elastic effect can be formally interpreted in terms of an extensional viscosity effect, despite the fundamental difference between the two mechanisms. However, when the extensional

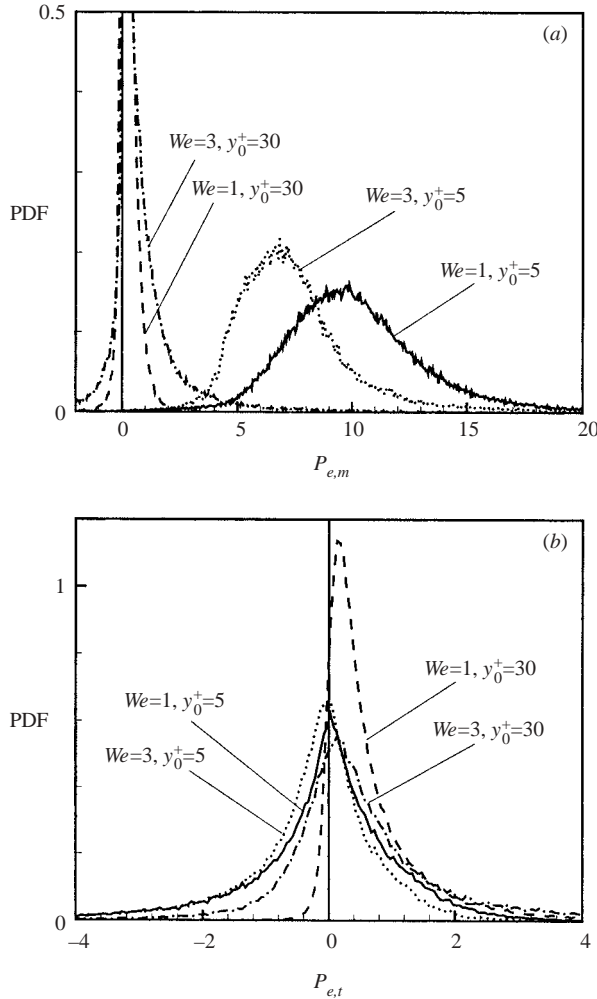


FIGURE 13. Probability density functions of $P_{e,m}$ and $P_{e,t}$ normalized by $u_{\tau_0}^3/\delta$ at $Re = 3000$: (a) $P_{e,m}$; (b) $P_{e,t}$.

We	$DR(\%)$	$P_{e,m}$		$P_{e,t}$	
		$y_0^+ \simeq 5$	$y_0^+ \simeq 30$	$y_0^+ \simeq 5$	$y_0^+ \simeq 30$
1	0	0	21	49	3
3	20	0	18	57	31

TABLE 2. Probabilities of negative $P_{e,m}$ and $P_{e,t}$ ($\int PDF(P_{e,m} < 0) dP_{e,m}$ and $\int PDF(P_{e,t} < 0) dP_{e,t}$) in per cent for $Re = 3000$.

viscosity alone is considered for polymer drag reduction, as done by Orlandi (1995) and den Toonder *et al.* (1997), the question of why the onset of drag reduction exists is very difficult to answer, which is the main reason why the elastic theory is introduced in the present study. After the onset, on the other hand, it is still premature to clearly identify which of the two mechanisms is dominant for drag reduction, because

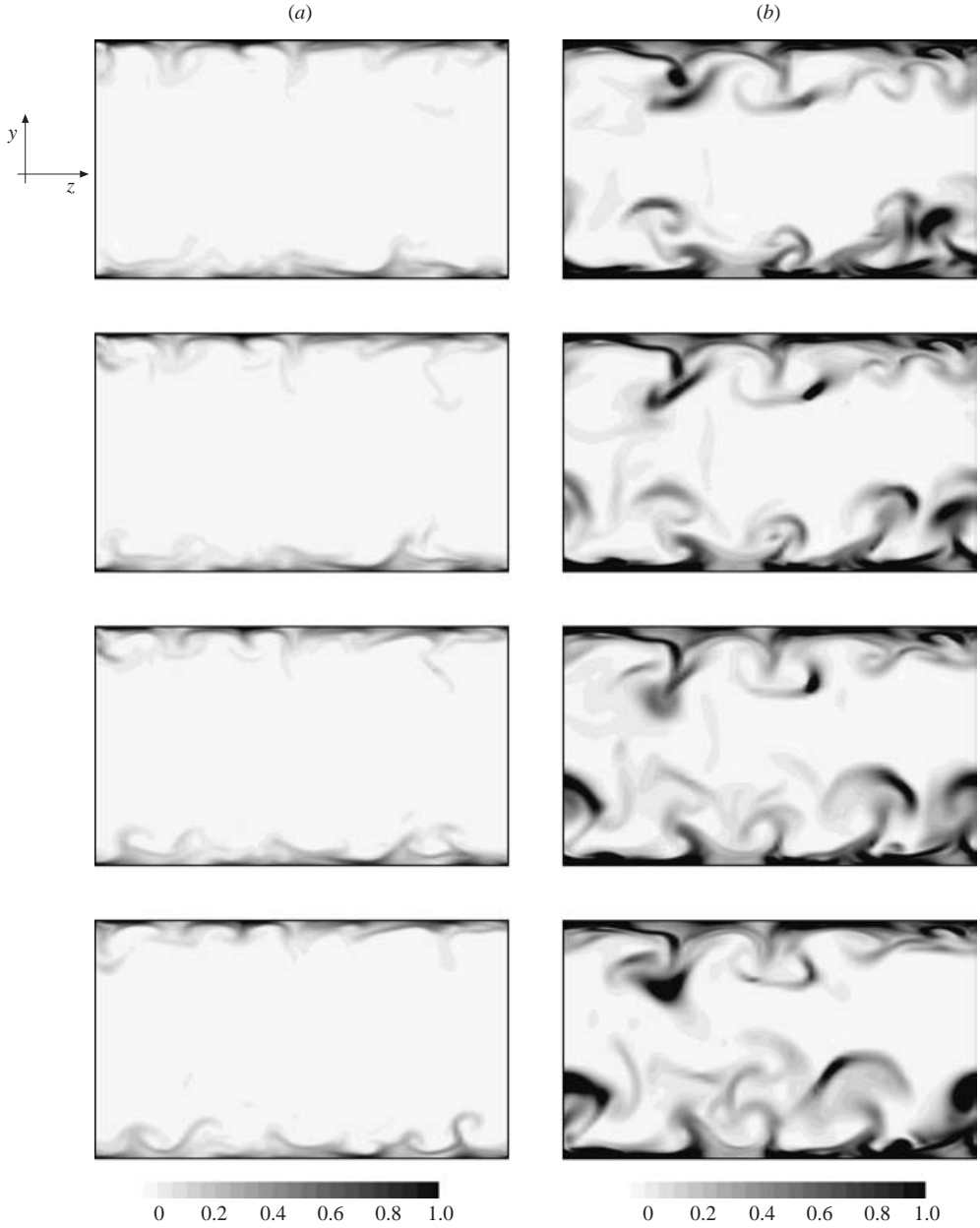


FIGURE 14. Time sequence of the instantaneous elastic energy k_p normalized by $u_{\tau_0}^2$ in a coordinate system moving with the structures at $Re = 3000$: (a) $We = 1$; (b) $We = 3$. The time interval between consecutive instants is 0.2.

the behaviour of turbulence in the presence of polymer is still largely unknown. In particular, the interaction between the polymer and the near-wall streamwise vortices should be an important future research subject.

Finally, it is certainly important to investigate the flow field with a non-homogeneous polymer concentration, especially in the wall-normal direction, for which it is very difficult to obtain physically meaningful results from the present

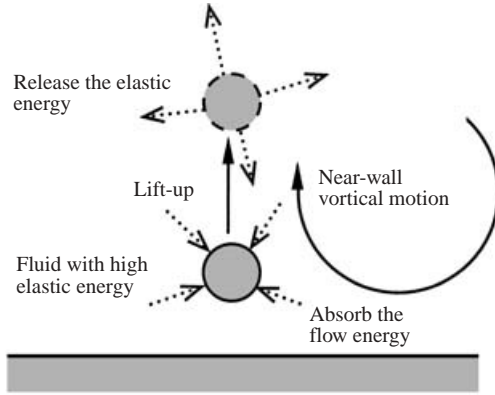


FIGURE 15. Schematic representation of the present drag-reduction mechanism.

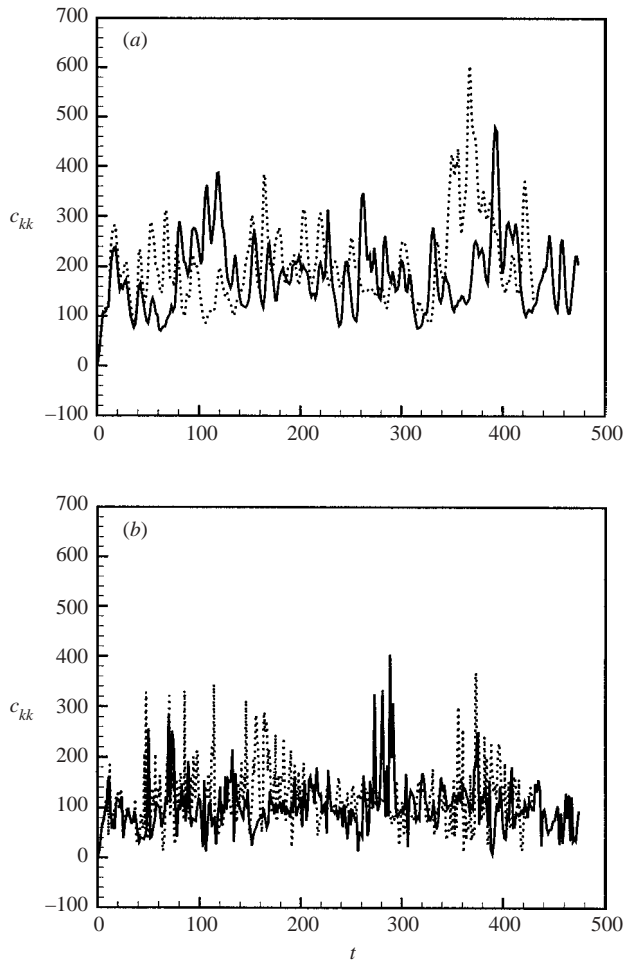


FIGURE 16. Time histories of the polymer stretch c_{kk} at $Re = 3000$ and $We = 2$: (a) $y_0^+ = 0.2$; (b) $y_0^+ = 10$. —, FENE-P model with $L^2 = 3600$; ·····, Oldroyd-B model.

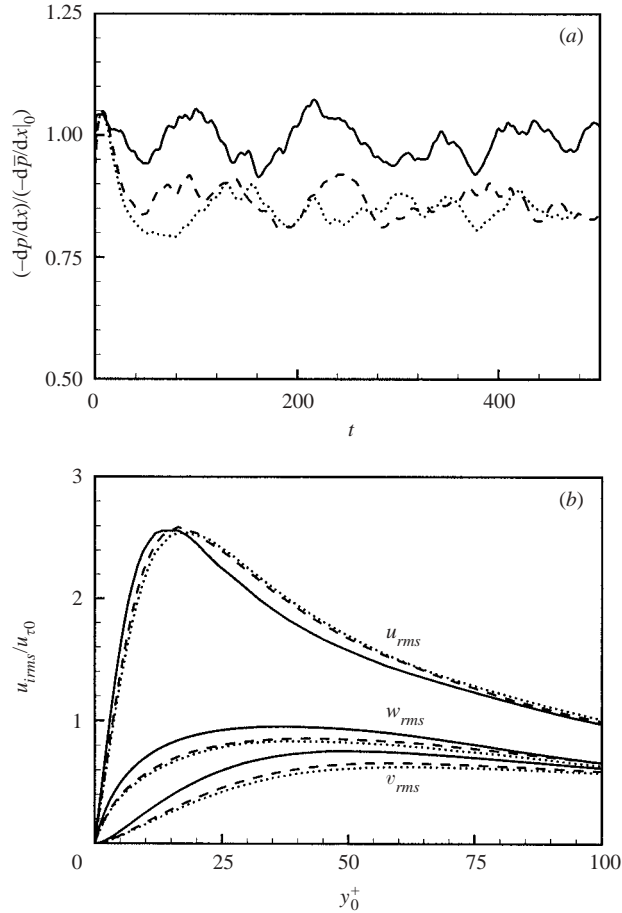


FIGURE 17. Comparison of the results from the Oldroyd-B and FENE-P models at $Re = 3000$ and $We = 2$: (a) time histories of the mean pressure gradient normalized by that of Newtonian fluid flow; (b) root-mean-square velocity fluctuations normalized by the wall-shear velocity u_{τ_0} . —, Newtonian; ---, Oldroyd-B model; ·····, FENE-P model with $L^2 = 3600$.

approach. However, the present drag-reduction mechanism suggests that the high concentration of polymer between the viscous sublayer and buffer layer should decrease drag significantly.

This study was supported by the Creative Research Initiatives and Korea Institute of Science & Technology Evaluation Planning (No. I-01-03-A-024) of the Korean Ministry of Science and Technology.

Appendix. Examination of unboundedness of polymer stretch in the Oldroyd-B model

Theoretically, the polymer stretch in the Oldroyd-B model does not have an upper bound. However, in a real flow field, this may not be the case because the time evolution of the polymer stretch is coupled with that of the shear rate. The FENE-P model becomes the Oldroyd-B model as $L^2 \rightarrow \infty$ (Bird *et al.* 1987), where L^2 is the dumbbell extensibility of the FENE-P model. Thus, the Oldroyd-B model is a limiting

case of the FENE-P model, and the FENE-P model behaves like the Oldroyd-B model when L^2 is sufficiently large.

In order to compare the magnitudes of the polymer stretch from both the FENE-P and Oldroyd-B models for the present flow, a computer code developed by Min *et al.* (2001) is used for the simulation with the FENE-P model. Figure 16 shows the time histories of the polymer stretch c_{kk} at $y_0^+ = 0.2$ and $y_0^+ = 10$. One can clearly see that the c_{kk} of the Oldroyd-B model has an upper bound in the present flow, and the boundedness of the FENE-P model with $L^2 = 3600$ is almost the same as that of the Oldroyd-B model. This value of L^2 corresponds roughly to a polystyrene molecule of molecular weight 10^6 (Dubief & Lele 2001). This figure also suggests that the FENE-P model with $L^2 = 1000$, adopted by Ptasinski *et al.* (2002), shows a similar behaviour to that of the Oldroyd-B model. Figures 17(a) and 17(b) show the time histories of the mean pressure gradient and the r.m.s. velocity fluctuations at $Re = 3000$ and $We = 2$, respectively. One can again see that the results of the Oldroyd-B model are in good agreement with those of the FENE-P model with $L^2 = 3600$.

REFERENCES

- BERMAN, N. S. 1977 Flow time scales and drag reduction. *Phys. Fluids* **20**, s168–s174.
- BIRD, R. B., CURTISS, C. F., ARMSTRONG, R. C. & HASSAGER, O. 1987 *Dynamics of Polymeric Liquids, Vol. 2, Kinetic Theory*. John Wiley & Sons.
- CADOT, O., BONN, D. & DOUADY, S. 1998 Turbulent drag reduction in a closed flow system: Boundary layer versus bulk effects. *Phys. Fluids* **10**, 426–436.
- CHOI, H., MOIN, P. & KIM, J. 1992 Turbulent drag reduction: studies of feedback control and flow over riblets. Rep. TF-55. Department of Mechanical Engineering, Stanford University, Stanford, CA.
- CHOI, H., MOIN, P. & KIM, J. 1993 Direct numerical simulation of turbulent flow over riblets. *J. Fluid Mech.* **255**, 503–539.
- CHOI, H., MOIN, P. & KIM, J. 1994 Active turbulence control for drag reduction in wall-bounded flows. *J. Fluid Mech.* **262**, 75–110.
- DIMITROPOULOS, C. D., SURESHKUMAR, R. & BERIS, A. N. 1998 Direct numerical simulation of viscoelastic turbulent channel flow exhibiting drag reduction: effect of the variation of rheological parameters. *J. Non-Newtonian Fluid Mech.* **79**, 433–468.
- DUBIEF, Y. & LELE, S. K. 2001 Direct numerical simulation of polymer flow. *Center for Turbulence Research Annual Briefs 2001*, pp. 197–208.
- DE GENNES, P. G. 1990 *Introduction to Polymer Dynamics*. Cambridge University Press.
- GOLDSHTIK, M. A., ZAMETALIN, V. V. & SHTERN, V. N. 1982 Simplified theory of the near-wall turbulent layer of Newtonian and drag-reducing fluids. *J. Fluid Mech.* **119**, 423–441.
- GYR, A & TSINOBER, A. 1997 On the rheological nature of drag reduction phenomena. *J. Non-Newtonian Fluid Mech.* **73**, 153–162.
- HERSHEY, H. C. & ZAKIN, J. L. 1967 A molecular approach to predicting the onset of drag reduction in the turbulent flow of dilute polymer solutions. *Chem. Engng Sci.* **22**, 1847–1856.
- HINCH, E. J. 1977 Mechanical models of dilute polymer solutions in strong flows. *Phys. Fluids* **20**, s22–s30.
- JIMÉNEZ, J. & MOIN, P. 1991 The minimal flow unit in near-wall turbulence. *J. Fluid Mech.* **225**, 213–240.
- JOSEPH, D. D. 1990 *Fluid Dynamics of Viscoelastic Liquids*. Springer.
- JOSEPH, D. D. & CHRISTODOULOU, C. 1993 Independent confirmation that delayed die swell is a hyperbolic transition. *J. Non-Newtonian Fluid Mech.* **48**, 225–235.
- LEE, D. & CHOI, H. 2001 MHD turbulent flow in a channel at low magnetic Reynolds number. *J. Fluid Mech.* **439**, 367–394.
- LELE, S. K. 1992 Compact finite difference schemes with spectral-like resolution. *J. Comput. Phys.* **103**, 16–42.
- LUMLEY, J. L. 1969 Drag reduction by additives. *Annu. Rev. Fluid Mech.* **1**, 367–384.

- LUMLEY, J. L. 1973 Drag reduction in turbulent flow by polymer additives. *J. Polymer Sci. Macromol. Rev.* **7**, 263–290.
- LUCHIK, T. S. & TIEDERMAN, W. G. 1988 Turbulent structure in low-concentration drag-reducing channel flows. *J. Fluid Mech.* **190**, 241–263.
- MASSAH, H. & HANRATTY, T. J. 1997 Added stresses because of the presence of FENE-P bead-spring chains in a random velocity field. *J. Fluid Mech.* **337**, 67–101.
- MIN, T., CHOI, H. & YOO, J. Y. 2002 Maximum drag reduction in a turbulent channel flow by polymer additives. *Proc. 55th Annual Meeting of APS DFD* **47**, No. 10, 53.
- MIN, T., YOO, J. Y. & CHOI, H. 2001 Effect of spatial discretization schemes on numerical solutions of viscoelastic fluid flows. *J. Non-Newtonian Fluid Mech.* **100**, 27–47.
- MOSER, R. D., KIM, J. & MANSOUR, N. N. 1999 Direct numerical simulation of turbulent channel flow up to $Re_\tau = 590$. *Phys. Fluids* **11**, 943–945.
- ORLANDI, P. 1995 A tentative approach to the direct simulation of drag reduction by polymers. *J. Non-Newtonian Fluid Mech.* **60**, 277–301.
- PINCUS, P. 1976 Excluded volume effects and stretched polymer-chains. *Macromolecules* **9**, 386–388.
- PTASINSKI, P. K., BOERSMA, B. J., NIEUWSTADT, F. T. M., VAN DER BRULE, B. H. A. A. & HUNT, J. C. R. 2002 Turbulent channel flow near maximum drag reduction: simulations, experiments and mechanisms. *J. Fluid Mech.* (submitted).
- SMITH, D. E. & CHU, S. 1998 Response of flexible polymers to a sudden elongational flow. *Science* **281**, 1335–1340.
- SREENIVASAN, K. R. & WHITE, C. M. 2000 The onset of drag reduction by dilute polymer additives, and the maximum drag reduction asymptote. *J. Fluid Mech.* **409**, 149–164.
- SURESHKUMAR, R., BERIS, A. N. & HANDLER, R. A. 1997 Direct numerical simulation of the turbulent channel flow of a polymer solution. *Phys. Fluids* **9**, 743–755.
- TABOR, M. & DE GENNES, P. G. 1986 A cascade theory of drag reduction. *Europhys. Lett.* **2**, 519–522.
- TOLSTYKH, A. I. & LIPAVSKII, M. V. 1998 On performance of methods with third- and fifth-order compact upwind differencing. *J. Comput. Phys.* **140**, 205–232.
- TOMS, B. A. 1949 Some observations on the flow of linear polymer solutions through straight tubes at large Reynolds numbers. *Proc. 1st Intl Congress on Rheology*, vol. 2, pp. 135–141. North-Holland.
- DEN TOONDER, J. M. J., HULSEN, M. A., KUIKEN, G. D. C. & NIEUWSTADT, F. T. M. 1997 Drag reduction by polymer additives in a turbulent pipe flow: numerical and laboratory experiments. *J. Fluid Mech.* **337**, 193–231.
- TULIN, M. P. 1966 Hydrodynamic aspects of macromolecular solutions. *Proc. 6th Symp. on Naval Hydrodynamics* (ed. R. D. Cooper & S. W. Doroff), pp. 3–18.
- VIRK, P. S. 1971 An elastic sublayer model for drag reduction by dilute solutions of linear macromolecules. *J. Fluid Mech.* **45**, 417–440.
- VIRK, P. S., MERRIL, E. W., MICKLEY, H. S., SMITH, K. A. & MOLLO-CHRISTENSEN, E. L. 1967 The Toms phenomenon-turbulent pipe flow of dilute polymer solutions. *J. Fluid Mech.* **30**, 305–328.
- WARHOLIC, M. D., MASSAH, H. & HANRATTY, T. J. 1999 Influence of drag-reducing polymers on turbulence: effects of Reynolds number, concentration and mixing. *Exps. Fluids* **27**, 461–472.
- WEI, T. & WILLMARTH, W. W. 1992 Modifying turbulent structure with drag-reducing polymer additives in turbulent channel flows. *J. Fluid Mech.* **245**, 619–641.